Inorganic Chemistry
Article

Inorg. Chem. **2009**, *48*, 7679–7690 **7679**
DOI: 10.1021/ic900415m

Behavior of P−Pt and P−Pd Bonds in Phosphido Complexes toward Electrophilic Fragments§

Ester Alonso,† Juan Forniés,*,† Consuelo Fortuño,*,† Agustí Lledós,*,‡ Antonio Martín,† and Ainara Nova‡

†*Departamento de Química Inorgánica and Instituto de Ciencia de Materiales de Aragón, Universidad de Zaragoza-CSIC, 50009 Zaragoza, Spain, and* ‡*Departament de Química, Universitat Autònoma de Barcelona, 08193 Bellaterra, Spain*

Received March 2, 2009

The reactions between the unsaturated 30-valence-electron-count $[(C_6F_5)_2Pt(\mu\text{-}PPh_2)_2M(PPh_3)]$ (M = Pt, Pd) and $[M'(OClO_3)PPh_3]$ (M′ = Ag, Au) yield the cationic trinuclear $[(C_6F_5)_2Pt(\mu\text{-}PPh_2)_2M(PPh_3)(M'PPh_3)][ClO_4]$ (M = Pt, Pd; M′ = Ag, Au), which displays Pt−M and M−M′ bonds. The X-ray structures of the complexes reveal that the core of the molecules is planar and the Pt−M and M−M′ distances point to the presence of Pt−M and M−M′ bonds. A computational study on the formation of these complexes and the analysis of the interaction between the binuclear fragment $[(C_6F_5)_2Pt(\mu\text{-}PPh_2)_2Pt(PPh_3)]$ and the cation $[Ag\ PPh_3]^+$ has been carried out on the basis of density functional theory and shows that the Ag center interacts weakly with M and P (PPh_2 ligand) atoms of the binuclear fragment.

Introduction

The reactivity of the anionic, neutral, or even cationic derivatives of platinum(II) toward silver centers to afford complexes displaying donor−acceptor Pt−Ag bonds has been well established.[1−11] In most of these complexes, the Pt−Ag bond is almost perpendicular to the platinum coordination plane, which allows a better overlap between the filled Pt(II) $5d_{z^2}$ and the vacant silver orbital. In some cases, the Ag(I) salts occasionally can act as an oxidant and remove two electrons from dinuclear platinum(II) complexes to give diplatinum(III) derivatives.[12−14]

In the course of our current research on palladium(II) and platinum(II) phosphido derivatives, we have reported the different behaviors of some diphenylphosphido derivatives toward silver(I) centers.[15−22] The anionic platinum(II) complex $[NBu_4]_2[(C_6F_5)_2Pt(\mu\text{-}PPh_2)_2Pt(C_6F_5)_2]$ reacts (Scheme 1a) with $AgClO_4$ (1:2 molar ratio), yielding Ag^0 and the neutral dinuclear platinum(III) derivative $[(C_6F_5)_2Pt(\mu\text{-}PPh_2)_2Pt(C_6F_5)_2]$,[15] while another anionic diphenylphosphido complex

§ Polynuclear Homo- or Heterometallic Palladium(II)−Platinum(II) Pentafluorophenyl Complexes Containing Bridging Diphenylphosphido Ligands. Part 26. For part 25, see ref 67.

*To whom correspondence should be addressed. E-mail: juan.fornies@unizar.es (J.F.).

(1) Forniés, J.; Martín, A. In *Metal Clusters in Chemistry*; Braunstein, P., Oro, L. A., Raithby, P. R., Eds.; Wiley-VCH: Weinheim, Germany, 1999; Vol. *1*, pp 417−443.
(2) Yam, W. W. W.; Yeung, P. K. Y.; Cheung, K. K. *Angew. Chem., Int. Ed. Engl.* **1996**, *35*, 739–740.
(3) Holthenrich, D.; Krumin, M.; Zangrando, E.; Pichierri, F.; Randaccio, L.; Lippert, B. *J. Chem. Soc., Dalton Trans.* **1995**, 3275–3279.
(4) Albinati, A.; Chaloupka, S.; Demartin, F.; Koetzle, T. F.; Ruegger, H.; Venanzi, L. M.; Wolfer, M. K. *J. Am. Chem. Soc.* **1993**, *115*, 169–175.
(5) Ebihara, M.; Tokoro, K.; Maeda, M.; Ogami, M.; Imaeda, K.; Sakurai, K.; Masuda, K.; Kawamura, T. *J. Chem. Soc., Dalton Trans.* **1994**, 3621–3635.
(6) Bender, R.; Bouaoud, S. E.; Braunstein, P.; Dusausoy, Y.; Merabet, N.; Raya, J.; Rouag, D. *J. Chem. Soc., Dalton Trans.* **1999**, 735–741.
(7) Archambault, C.; Bender, R.; Braunstein, P.; Dusausoy, Y. *J. Chem. Soc., Dalton Trans.* **2002**, 4084–4090.
(8) Forniés, J.; Martín, A.; Navarro, R.; Sicilia, V.; Villarroya, P.; Orpen, A. G. *J. Chem. Soc., Dalton Trans.* **1998**, 3721–3726.
(9) Janzen, D. E.; Mehne, L. F.; VanDerveer, D. G.; Grant, G. J. *Inorg. Chem.* **2005**, *44*, 8182–8184.
(10) Oberbeckmann-Winter, N.; Morise, X.; Braunstein, P.; Welter, R. *Inorg. Chem.* **2005**, *44*, 1391–1403.
(11) Song, H.-B.; Zhang, Z.-Z.; Hui, Z.; Che, C.-M.; Mak, T. C. W. *Inorg. Chem.* **2002**, *41*, 3146–3154.
(12) Rendina, L. M.; Hambley, T. W. In *Comprehensive Coordination Chemistry II*; McCleverty, J. A., Meyer, T. J., Eds.; Elsevier Inc.: San Diego, CA, 2004; Vol. *6*.
(13) Lippert, B.; Schollhorn, H.; Thewalt, U. *Inorg. Chem.* **1987**, *26*, 1736–1741.
(14) Oskui, B.; Sheldrick, W. S. *Eur. J. Inorg. Chem.* **1999**, *8*, 1325–1333.
(15) Alonso, E.; Casas, J. M.; Cotton, F. A.; Feng, X. J.; Forniés, J.; Fortuño, C.; Tomás, M. *Inorg. Chem.* **1999**, *38*, 5034–5040.
(16) Alonso, E.; Casas, J. M.; Forniés, J.; Fortuño, C.; Martín, A.; Orpen, A. G.; Tsipis, C. A.; Tsipis, A. C. *Organometallics* **2001**, *20*, 5571–5582.
(17) Forniés, J.; Fortuño, C.; Ibáñez, S.; Martín, A.; Tsipis, A. C.; Tsipis, C. A. *Angew. Chem., Int. Ed.* **2005**, *44*, 2407–2410.
(18) Forniés, J.; Fortuño, C.; Gil, R.; Martín, A. *Inorg. Chem.* **2005**, *44*, 9534–9541.
(19) Berenguer, J. R.; Chaouche, N.; Forniés, J.; Fortuño, C.; Martín, A. *New J. Chem.* **2006**, *30*, 473–478.
(20) Alonso, E.; Forniés, J.; Fortuño, C.; Martín, A.; Orpen, A. G. *Organometallics* **2003**, *22*, 5011–5019.
(21) Falvello, L. R.; Forniés, J.; Fortuño, C.; Durán, F.; Martín, A. *Organometallics* **2002**, *21*, 2226–2234.
(22) Forniés, J.; Fortuño, C.; Ibáñez, S.; Martín, A. *Inorg. Chem.* **2008**, *47*, 5978–5987.

Published on Web 07/23/2009

Scheme 1

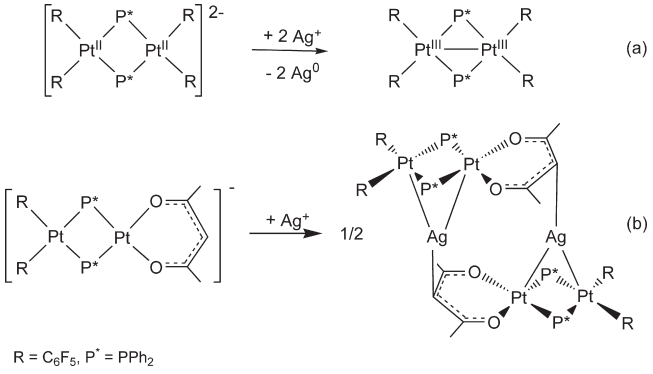

$[NBu_4][(C_6F_5)_2Pt(\mu\text{-}PPh_2)_2Pt(acac)]$ affords (Scheme 1b) the neutral hexanuclear cluster $[\{AgPt_2(\mu\text{-}PPh_2)_2(C_6F_5)_2(acac)\}_2]$, which shows donor−acceptor Pt−Ag bonds.[20] The coordination of two pentafluorophenyl groups or an acetylacetonate ligand to the fragment "$(C_6F_5)_2Pt(\mu\text{-}PPh_2)_2Pt$" results in a very different behavior of these anionic complexes.

With the aim of studying the influence of the groups bonded to the fragment "$(C_6F_5)_2Pt(\mu\text{-}PPh_2)_2Pt$" on their reactions toward silver centers, we have studied the behavior of a neutral unsymmetrical platinum(II) derivative $[(C_6F_5)_2Pt(\mu\text{-}PPh_2)_2Pt(PPh_3)_2]$,[21] **1**. According to our previous experience, it is not possible to establish a priori if a redox process that would render a cationic Pt(III)−Pt(III) complex (as in Scheme 1a) or a Lewis acid−base reaction (as in Scheme 1b) yielding clusters with Pt−Ag bonds would function. In addition, in the latter case, the dinuclear platinum complex could behave as a monodentate ligand through the more anionic metal center, or as a bidentate metalloligand using the two platinum centers as donor atoms. However, the result of this reaction is rather different from the expected one since, although the Ag^+ coordinates to the binuclear complex through a donor−acceptor interaction, the resulting complex displays a rather different structure. This fact prompted us to carry out a more complete study on the behavior of the homo- or heterodinuclear Pt/Pd complexes toward silver or gold centers. The results of this study have also been fully interpreted in the light of density functional theory (DFT) calculations.

Results and Discussion

1. Synthesis of $[\{M'PtM(\mu\text{-}PPh_2)_2(C_6F_5)_2(PPh_3)_2\}]^+$ Cations (M = Pt or Pd, M′ = Ag or Au). The reaction of $[(C_6F_5)_2Pt(\mu\text{-}PPh_2)_2Pt(PPh_3)_2]$, **1**, with $AgClO_4$ (1:1 molar ratio) in CH_2Cl_2 affords (Scheme 2) the cationic derivative $[\{AgPt_2(\mu\text{-}PPh_2)_2(C_6F_5)_2(PPh_3)_2\}][ClO_4]$, **2**-$[ClO_4]$. The identity of **2**$[ClO_4]$ has been established by an X-ray study (see below) that shows cation **2** to be a structurally different trinuclear cluster in which the Pt···Ag vector is not perpendicular to the coordination plane of any of the platinum centers but rather on the same plane. The reaction could be considered as the insertion of Ag^+ into the Pt−PPh_3 bond, giving rise to the formation of Pt−Ag and Ag−PPh_3 bonds. The electronic requirements of this platinum center are completed by the formation of a Pt−Pt bond, while those of the silver center are afforded by an interaction with a P atom of a PPh_2 group.

Scheme 2

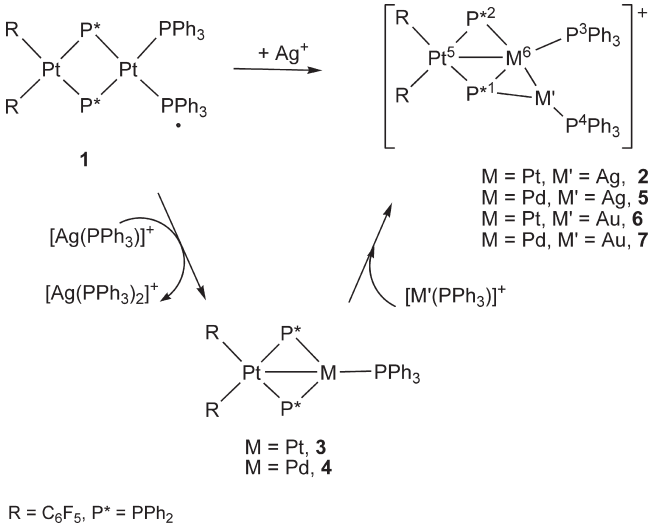

This result prompts us to study the behavior of **1** toward the $AgPPh_3^+$ fragment with the aim of synthesizing a cationic cluster $[AgPt_2(\mu\text{-}PPh_2)_2(C_6F_5)_2(PPh_3)_3][ClO_4]$ with one or two typical donor−acceptor Pt−Ag bonds in an analogous process to the one which renders $[AgMPt(\mu\text{-}PPh_2)_2(C_6F_5)_2(acac)(PPh_3)]$.[20] Nevertheless, the reaction of CH_2Cl_2 solutions of **1** with $[Ag(OClO_3)PPh_3]$ in a 1:1 molar ratio produces (^{31}P NMR spectroscopy) a mixture of **1**, **2**$[ClO_4]$, and $[Ag(PPh_3)_2]^+$. When the molar ratio used is 1:2, only the trinuclear cluster **2**$[ClO_4]$ and $[Ag(PPh_3)_2]^+$ are obtained. From the latter reaction, it can be construed that the $[Ag(PPh_3)]^+$ fragment behaves as a PPh_3 scavenger toward **1**, affording $[Ag(PPh_3)_2]^+$ and the previously reported 30-electron valence skeleton complex $[(C_6F_5)_2Pt(\mu\text{-}PPh_2)_2Pt(PPh_3)]$,[23] **3**. This, once it has formed, reacts with equimolar amounts of $[Ag(PPh_3)]^+$, yielding the trinuclear cluster **2**$[ClO_4]$ (Scheme 2). The reaction of **1** with $[Ag(PPh_3)]^+$ in a 1:1 molar ratio indicates that the fragment $[Ag(PPh_3)]^+$ prefers coordination to **3** rather than acting as a PPh_3 scavenger of **1**. In order to confirm this proposal, we have added $[Ag(OClO_3)PPh_3]$ to a red CH_2Cl_2 solution of **3** (1:1 molar ratio). Instantaneously, the color of the solution changes to orange, and after the adequate workup, complex **2**$[ClO_4]$ is obtained (94% yield).

Taking into account the ease with which the trinuclear cluster **2**$[ClO_4]$ is obtained by connecting the two fragments, **3** and $[Ag(PPh_3)]^+$, and given the difficulty that we have previously experienced in obtaining complexes with Pd−Ag bonds,[1,24−27] we have carried out a similar reaction but using the unsaturated Pt(II)−Pd(II) diphenylphosphido compound $[(C_6F_5)_2Pt(\mu\text{-}PPh_2)_2Pd(PPh_3)]$,[23]

(23) Falvello, L. R.; Forniés, J.; Fortuño, C.; Martínez, F. *Inorg. Chem.* **1994**, *33*, 6242–6246.
(24) Falvello, L. R.; Forniés, J.; Martín, A.; Sicilia, V.; Villarroya, P. *Organometallics* **2002**, *21*, 4604–4610.
(25) Forniés, J.; Martínez, F.; Navarro, R.; Urriolabeitia, E. *Organometallics* **1996**, *15*, 1813–1819.
(26) Usón, R.; Forniés, J.; Tomás, M.; Ara, I.; Casas, J. M.; Martín, A. *J. Chem. Soc., Dalton Trans.* **1991**, 2253–2264.
(27) Braunstein, P.; Frison, U.; Oberbeckmann-Winter, N.; Morise, X.; Messaoudi, A.; Bénard, M.; Rohmer, M.-M.; Welter, R. *Angew. Chem., Int. Ed. Engl.* **2004**, *43*, 6120–6125.

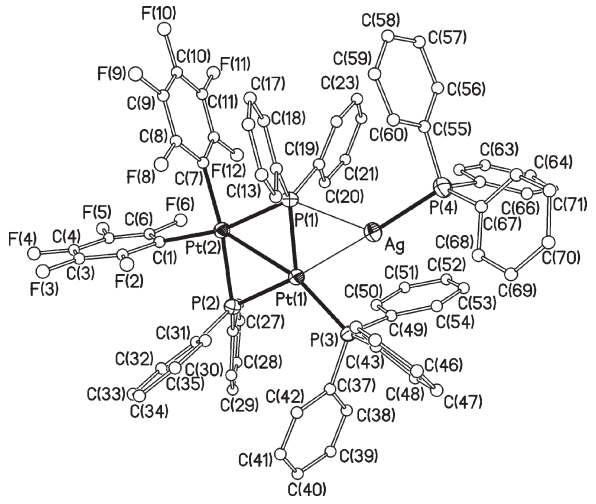

Figure 1. Crystal structure of the cation **2**.

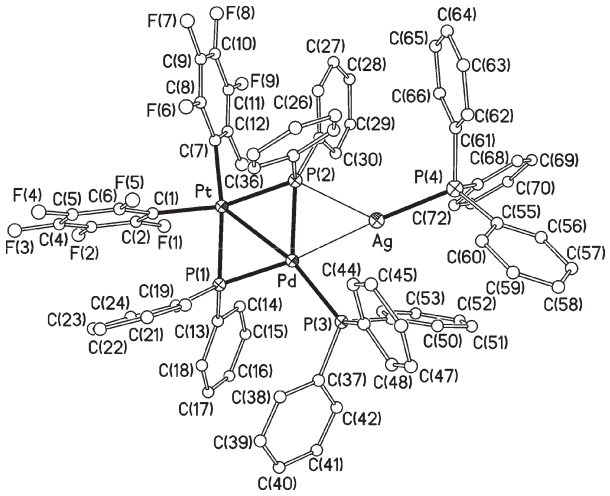

Figure 2. Crystal structure of the cation **5**.

4, as starting material in order to prepare a complex with a Pd−Ag bond. The reaction gives (Scheme 2) the analogous cluster $[AgPdPt(\mu\text{-}PPh_2)_2(C_6F_5)_2(PPh_3)_2][ClO_4]$, **5**$[ClO_4]$. This process and the type of interaction between the Pt or Pd and Ag fragments (we will discuss later) are similar to that reported by Braunstein et al.,[28] $[\{AuPt(\mu\text{-}PPh_2)(PPh_3)_2\}_2]^{2+}$, although in the latter the formal oxidation state of the Pt center is I, while in the complexes here reported, the Pd or Pt centers are in formal oxidation state II.

It is remarkable that the synthesis of complexes with a donor−acceptor M−Ag (M = Pt, Pd) bond would seem to be very difficult for M = Pd,[1,24−26,29] and only a few complexes in which the Pd−Ag distance is less than 2.9 Å have been reported.[20,27,30,31] In the same context, the cationic complex $[PtAg(\mu\text{-dcpm})_2(CN)_2]ClO_4$ shows a Pt(II)−Ag(I) interaction, the Pt···Ag vector being perpendicular to the coordination plane of platinum, while the analogous Pd−Ag complex has not been reported.[32]

A similar synthetic procedure enables the preparation of the corresponding gold complexes $[AuMPt(\mu\text{-}PPh_2)_2(C_6F_5)_2(PPh_3)_2][ClO_4]$ (M = Pt, **6**$[ClO_4]$, or Pd, **7**$[ClO_4]$) by reacting complexes **3** (or **4**) with $[Au(PPh_3)]^+$ (Scheme 2).

2. Characterization of $[\{M'PtM(\mu\text{-}PPh_2)_2(C_6F_5)_2(PPh_3)_2\}]^+$ cations (M = Pt or Pd, M′ = Ag or Au). The crystal structures of the complex cations **2**, **5**, and **6** are shown in Figures 1−3, and selected structural data are listed in Tables 1−3, respectively. The structures of the three cations are very similar and will be described together. For descriptive purposes, the structures can be regarded as the union of "$(C_6F_5)_2Pt(\mu\text{-}PPh_2)_2M(PPh_3)$" (M = Pt(II) for **2** and **6** and Pd(II) for **5**) with "$M'(PPh_3)^+$" (M′ = Ag for **2** and **5** and Au in the case of **6**). In the first subunit, the Pt_2 or PtPd and the atoms directly bonded to them are essentially located in the same plane, in a similar structural situation to that presented in $[\{AuPt(\mu\text{-}PPh_2)(PPh_3)_2\}_2]^{2+}$,[28] a complex formed by the interaction of the platinum(I) dinuclear derivative $[\{Pt(\mu\text{-}PPh_2)(PPh_3)\}_2]$ with two $\{Au(PPh_3)\}^+$ fragments. The

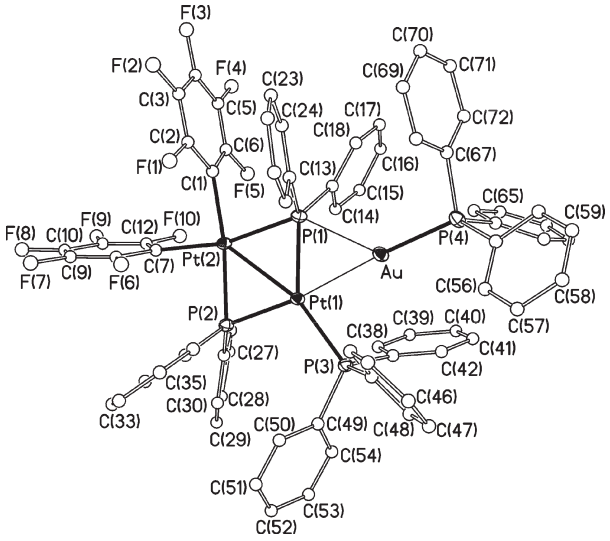

Figure 3. Crystal structure of the cation **6**.

Table 1. Selected Bond Distances (Å) and Angles (deg) for $[AgPt_2(\mu\text{-}PPh_2)_2(C_6F_5)_2(PPh_3)_2][ClO_4]\cdot 2.5CH_2Cl_2$ (**2**$[ClO_4]\cdot 2.5CH_2Cl_2$)[a]

Pt(1)−P(2)	2.241(2) [*2.346*]	Pt(2)−P(2)	2.298(2) [*2.337*]
Pt(1)−Pt(2)	2.7052(5) [*2.880*]	Ag−P(1)	2.686(2) [*2.750*]
Pt(2)−C(7)	2.094(9) [*2.098*]	Pt(1)−P(1)	2.280(2) [*2.413*]
Ag−P(4)	2.402(3) [*2.477*]	Pt(2)−C(1)	2.061(10) [*2.089*]
Pt(1)−P(3)	2.252(2) [*2.306*]	Pt(2)−P(1)	2.368(2) [*2.380*]
Pt(1)−Ag	2.7076(9) [*2.763*]		
P(2)−Pt(1)−P(3)	107.96(8) [*107.3*]	P(2)−Pt(1)−P(1)	110.31(8) [*104.4*]
P(3)−Pt(1)−P(1)	141.33(9) [*147.5*]	P(2)−Pt(1)−Ag	174.78(6) [*168.1*]
P(3)−Pt(1)−Ag	77.17(6) [*84.3*]	P(1)−Pt(1)−Ag	64.49(6) [*63.8*]
C(1)−Pt(2)−C(7)	84.1(4) [*82.5*]	C(1)−Pt(2)−P(2)	87.5(3) [*87.9*]
C(7)−Pt(2)−P(2)	171.6(2) [*166.2*]	C(1)−Pt(2)−P(1)	166.8(3) [*162.6*]
C(7)−Pt(2)−P(1)	83.0(2) [*85.8*]	P(2)−Pt(2)−P(1)	105.32(8) [*105.7*]
P(4)−Ag−P(1)	127.50(8) [*143.2*]	P(4)−Ag−Pt(1)	176.39(7) [*163.8*]
P(1)−Ag−Pt(1)	50.01(5) [*51.9*]	Pt(1)−P(1)−Pt(2)	71.16(7) [*73.9*]
Pt(1)−P(1)−Ag	65.50(6) [*64.3*]	Pt(1)−P(2)−Pt(2)	73.16(7) [*75.9*]

[a] In brackets, BLYP/ONIOM optimized geometry of **2**.

(28) Bender, R.; Braunstein, P.; Dedieu, A.; Dusausoy, Y. *Angew. Chem., Int. Ed. Engl.* **1989**, *28*, 923–925.
(29) van Leeuven, P. W. N. M.; Zuideveld, M. A.; Swennenhuis, B. H. G.; Freixa, Z.; Kamer, P. C. J.; Goubitz, K.; Fraanje, J.; Lutz, M.; Spek, A. L. *J. Am. Chem. Soc.* **2003**, *125*, 5523–5539.
(30) Liu, Y.; Lee, K. H.; Vittal, J. J.; Hor, T. S. A. *J. Chem. Soc., Dalton Trans.* **2002**, 2747–2751.
(31) Kickman, J. E.; Loeb, J. J. *Organometallics* **1995**, *14*, 3584–3587.
(32) Xia, B.-H.; Zhang, H.-X.; Che, C.-M.; Leung, K.-H.; Phillips, D. L.; Zhu, N.; Zhou, Z.-Y. *J. Am. Chem. Soc.* **2003**, *125*, 10362–10374.

Table 2. Selected Bond Distances (Å) and Angles (deg) for $[AgPtPd(\mu\text{-}PPh_2)_2(C_6F_5)_2(PPh_3)_2][ClO_4]\cdot 4CH_2Cl_2$ (**5**[**ClO**$_4$]$\cdot 4CH_2Cl_2$)

Pt−C(7)	2.066(5)	Pd−P(2)	2.3060(14)
Pt−P(2)	2.3447(13)	Ag−P(2)	2.6037(14)
Pd−P(3)	2.2686(14)	Pt−P(1)	2.2959(14)
Ag−P(4)	2.4049(14)	Pd−P(1)	2.2384(14)
Pt−C(1)	2.066(5)	Pd−Ag	2.6829(6)
Pt−Pd	2.6760(4)		
C(7)−Pt−C(1)	86.9(2)	C(7)−Pt−P(1)	169.24(14)
C(1)−Pt−P(1)	84.60(14)	C(7)−Pt−P(2)	82.99(14)
C(1)−Pt−P(2)	164.78(14)	P(1)−Pt−P(2)	106.60(5)
P(1)−Pd−P(3)	111.82(5)	P(1)−Pd−P(2)	109.92(5)
P(3)−Pd−P(2)	138.07(5)	P(1)−Pd−Ag	169.07(4)
P(3)−Pd−Ag	76.74(4)	P(2)−Pd−Ag	62.38(4)
P(4)−Ag−P(2)	131.59(5)	P(4)−Ag−Pd	173.45(4)
P(2)−Ag−Pd	51.70(3)	Pd−P(1)−Pt	72.32(4)
Pd−P(2)−Ag	65.92(4)		

Table 3. Selected Bond Distances (Å) and Angles (deg) for $[AuPt_2(\mu\text{-}PPh_2)_2(C_6F_5)_2(PPh_3)_2][ClO_4]\cdot 2.5CH_2Cl_2$ (**6**[**ClO**$_4$]$\cdot 2.5CH_2Cl_2$)

Pt(1)−P(2)	2.2367(9)	Pt(2)−P(2)	2.2915(9)
Pt(1)−Au	2.6710(2)	Au−P(1)	2.5807(10)
Pt(2)−C(1)	2.079(4)	Pt(1)−P(1)	2.2791(9)
Au−P(4)	2.2914(10)	Pt(2)−C(7)	2.073(4)
Pt(1)−P(3)	2.2569(9)	Pt(2)−P(1)	2.3600(9)
Pt(1)−Pt(2)	2.6982(2)		
P(2)−Pt(1)−P(3)	106.99(3)	P(2)−Pt(1)−P(1)	110.19(3)
P(3)−Pt(1)−P(1)	142.52(3)	P(2)−Pt(1)−Au	172.44(2)
P(3)−Pt(1)−Au	80.56(2)	P(1)−Pt(1)−Au	62.25(2)
C(7)−Pt(2)−C(1)	83.99(14)	C(7)−Pt(2)−P(2)	87.59(10)
C(1)−Pt(2)−P(2)	171.52(10)	C(7)−Pt(2)−P(1)	166.32(10)
C(1)−Pt(2)−P(1)	82.94(10)	P(2)−Pt(2)−P(1)	105.53(3)
P(4)−Au−P(1)	131.55(3)	P(4)−Au−Pt(1)	175.36(3)
P(1)−Au−Pt(1)	51.41(2)	Pt(1)−P(1)−Pt(2)	71.10(3)
Pt(1)−P(1)−Au	66.34(3)		

intermetallic Pt−M distances are very similar in the three complexes (Pt(1)−Pt(2) = 2.705(1) Å for **2**, Pt−Pd = 2.676(1) Å for **5**, and Pt(1)−Pt(2) = 2.698(1) Å for **6**), indicating in all cases the presence of Pt−M (M = Pt, Pd) bonds (30 e^- valence skeleton). Accordingly, the Pt−(μ-P)−M angles are narrow (Pt(1)−P(1)−Pt(2) = 71.17(6)° and Pt(1)−P(2)−Pt(2) = 73.16(7)° for **2**, Pd−P(1)−Pt = 72.32(4)° and Pd−P(2)−Pt = 70.25(4)° for **5**, and Pt(1)−P(1)−Pt(2) = 71.10(3)° and Pt(1)−P(2)−Pt(2) = 73.14(3)° for **6**). Pt(2) in **2** and **6** and Pt in **5** lie in the center of a square-planar environment somewhat distorted due to the opening of the P−M−P angle (105.32(8)° for **2**, 106.60(5)° for **5**, and 106.99(3)° for **6**), a commonly observed effect in these $M(\mu\text{-}PPh_2)_2M'$ systems with metal−metal bonds. The environments of Pt(1) (**2**, **6**) and Pd (**5**) are more complex, considering the presence of three ligands, the silver or gold centers, and the Pt−M bond, and are analogous to that found in $[\{AuPt(\mu\text{-}PPh_2)(PPh_3)_2\}_2]^{2+}$.[28]

The silver atom is bonded to the Pt(1) and P(1) atoms in **2**, and to the Pd and P(2) atoms in **5**. The M−Ag distances (2.707(1) Å for **2** and 2.683(6) Å for **5**) are at the lower end of the range found for Pt/Pd−Ag bonds.[1,20] Nevertheless, the geometry of the complexes containing this kind of Pt/Pd→Ag bond is usually very different from that depicted by **2** or **5**. In the former, the Pt−Ag line forms small angles perpendicular to the best square plane of the Pt atom; that is, the Pt−Ag line tends to be perpendicular to the square plane. The geometric disposition found for **2** and **5** is such that the Ag atom lies nearly in the same plane as the Pt(μ-P)$_2$M (M = Pt (**2**), Pd (**5**)) core (the dihedral angles between the best Pt(μ-P)$_2$M planes and the Ag−M−(μ-P) plane are 1.8° for **2** and 14.1° for **5**). Furthermore the Ag−(μ-P) distance (2.686(2) Å for **2** and 2.604(1) Å for **5**) is clearly longer than any usual Ag−P bond, and even longer than the M−P distances found in complexes prepared by us containing μ^3-PPh_2 ligands.[33−36] The situation of the Au center in **6** is very similar. The Au atom is bonded to Pt(1) and P(1) (distances are 2.671(1) Å and 2.581(1) Å, respectively) and completes its coordination sphere with the P(4) atom from a PPh_3 ligand. The coordination environment of the gold atom is planar and coplanar to the Pt(1)−Pt(2)−P(1)−P(2) plane (the dihedral angle is only 0.4°). This part of the cation is very similar to that found in $[\{AuPt(\mu\text{-}PPh_2)(PPh_3)_2\}_2]^{2+}$,[28] the main difference being that, in **6**, the core is planar while in $[\{AuPt(\mu\text{-}PPh_2)(PPh_3)_2\}_2]^{2+}$ it is displayed as a hammock skeleton. All of these geometric parameters indicate a three-center−two-electron (3c−2e) bond system involving the electron pair of the Pt/Pd−P bond and the Ag/Au centers (vide infra).

The coordination sphere of the Ag (**2**, **5**) or Au atoms (**6**) is flat and is completed by a PPh_3 ligand. This ligand forms an almost straight line with Pt(1) in **2** (P(4)−Ag−Pt(1) = 176.39(7)°) and **6** (P(4)−Au−Pt(1) = 175.36(3)°) and with Pd (P(4)−Ag−Pd = 173.45(4)°) in **5**. This angle could indicate that the interaction between the platinum moiety and the $[M'PPh_3]^+$ fragment is only due to a Pt/Pd→Ag/Au bond, with the Ag or Au centers thus displaying a typical linear coordination. However, and as is demonstrated later, Pt/Pd, P and Ag/Au centers participate in the interaction, and the linearity of the Pt/Pd−Ag/Au−PPh_3 could be due to the steric hindrance of the PPh_3 ligands. Determination of the crystal structure of $[AuPtPd(\mu\text{-}PPh_2)_2(C_6F_5)_2(PPh_3)_2][ClO_4]$ (**7**[ClO_4]) was also attempted, but in this case the quality of the crystal sample precluded completion of the refinement of the diffraction data obtained. Nevertheless, the position of all of the atoms of the complex, as well as its connectivity, was unambiguously established, revealing the fact that **7** is isostructural to **2**, **5**, and **6**.

The $^{31}P\{^1H\}$ NMR spectra of **2**[ClO_4], **5**[ClO_4], **6**[ClO_4], and **7**[ClO_4] ($CDCl_3$ solution) show four signals, and all data are given in the Experimental Section. Signals due to P atoms of phosphido ligands appear in the low-field region, in agreement with the presence of PPh_2 groups bridging two platinum or palladium centers joined by a metal−metal bond.[36−41] Nevertheless, the two values of the chemical shift for these two P atoms within each cluster are very different, suggesting remarkably different chemical environments for the two nuclei due

(33) Alonso, E.; Forniés, J.; Fortuño, C.; Martín, A.; Orpen, A. G. *Organometallics* **2003**, *22*, 2723–2728.
(34) Alonso, E.; Forniés, J.; Fortuño, C.; Martín, A.; Orpen, A. G. *Chem. Commun.* **1996**, 231–232.
(35) Falvello, L. R.; Forniés, J.; Fortuño, C.; Martín, A.; Martínez-Sariñena, A. P. *Organometallics* **1997**, *16*, 5849–5856.
(36) Alonso, E.; Forniés, J.; Fortuño, C.; Martín, A.; Orpen, A. G. *Organometallics* **2000**, *19*, 2690–2697.
(37) Carty, A. J.; MacLaughlin, S. A.; Nucciarone, D. *Phosphorus-31 NMR Spectroscopy in Stereochemical Analysis*; VCH: New York, 1987.
(38) Ara, I.; Chaouche, N.; Forniés, J.; Fortuño, C.; Kribii, A.; Tsipis, A. C. *Organometallics* **2006**, *25*, 1084–1091.
(39) Forniés, J.; Fortuño, C.; Ibáñez, S.; Martín, A. *Inorg. Chem.* **2006**, *45*, 4850–4858.
(40) Chaouche, N.; Forniés, J.; Fortuño, C.; Kribii, A.; Martín, A.; Karipidis, P.; Tsipis, A. C.; Tsipis, C. A. *Organometallics* **2004**, *23*, 1797–1810.
(41) Mastrorilli, P. *Eur. J. Inorg. Chem.* **2008**, 4835–4850.

to the different coordination mode of both diphenylphosphido groups in the complexes. The displacement of the chemical shift toward high field on going from the μ_2-PR_2 to a μ_3-PR_2 system in a complex which shows both types of coordination has been observed previously,[42,43] and we have also observed this trend in our Pt/Pd clusters displaying a μ_3-PPh_2 group.[33−36] Moreover, a decrease in the δP value is observed in the 3c−2e P−H−M system with respect to the M(μ-P^{t}Bu$_2$)M one in complexes $[Pd_2(\mu\text{-}P^tBu_2)(\mu\text{-}P^tBu_2H)(P^tBu_2H)_2]^+$ [44,45] and $[Pt_2(\mu\text{-}P^tBu_2)(\mu\text{-}P^tBu_2H)(\eta^2\text{-}CH_2{=}CH_2)_2]^+$.[46] Thus, the signal due to the μ_3-PPh_2 group, P^1 (see Scheme 2 for atom numbering), is unambiguously assigned, $\delta P^1 \ll \delta P^2$. The observation of $^{107/109}$Ag−P scalar couplings for complexes **2** and **5** further confirms such assignments.

In the cationic clusters of gold **6** and **7**, the ^{31}P NMR signals at 295 K are well resolved, and the relevant coupling constants afford reliable information about the behavior in solution of the (μ-P)−Pt and (μ-P)−Pd bonds toward electrophiles.

The coupling constant between P^4 and P^2 through three bonds in a pseudolinear P^2−M−Au−P^4 system (45 Hz in **6**, 35 Hz in **7**) is smaller than the coupling between P^4 and P^1 (90 Hz in **6**, 138 Hz in **7**), in agreement with the presence of the P^1−Au interaction in solution.

In the cationic clusters of silver **2** and **5**, the ^{31}P NMR signals at 295 K are very broad. On lowering the temperature down to 213 K, the fine structure for the P signals becomes apparent. However, while the NMR features for P^3 are directly assessable from the $^{31}P\{^1H\}$ NMR spectrum, the P^1, P^2, and P^4 signals do not allow the precise assignment of all of the coupling constants, due to the presence of ^{31}P−^{31}P and ^{19}F−^{31}P (for P^1 and P^2) or ^{31}P−^{31}P, ^{107}Ag−^{31}P, and ^{109}Ag−^{31}P (for P^4) couplings of comparable entities. It is noteworthy that no clear ^{195}Pt satellites flank the P^4 signal of **2**, suggesting a dynamic behavior of the coordinated Ag(PPh_3) fragment (vide infra). The P^3 signals appear as doublets of doublets due to couplings with P^1 ($^2J_{P^3,P^1}$ = 153 Hz for **2** and 106 Hz for **5**) and P^2 ($^2J_{P^3,P^2}$ = 8 Hz for **2** and 11 Hz for **5**).

It is noteworthy that the chemical shifts of P^2 and P^1 in **2** ($AgPt_2$) are almost identical to those in **6** ($AuPt_2$). The same holds true for **5** (AgPdPt) and **7** (AuPdPt). These results indicate that the electronic environments of these P atoms do not depend on the nature of the incoming electrophile ($AgPPh_3^+$ or $AuPPh_3^+$) but on the nature of the starting dinuclear fragment, **3** (Pt_2) or **4** (PtPd). In each case, the δP value of the P^1 atom is less than that of the P^2 atom; the differences of these values ($\delta P^2 - \delta P^1$) are 81.9 and 74 ppm for the diplatinum complexes **2** and **6**, respectively, while this difference is greater, 133.4 and 136.0 ppm, for the palladium complexes **5** and **7**, respectively. Assuming that this decrease in the chemical shift is related to the 2e−3c bonding mode, we can conclude that there is a greater interaction of the (μ-P)−Pd bond than the (μ-P)−Pt bond with the electrophiles $M'PPh_3^+$. The Ag−M and Ag−(μ-P) bond lengths (See Tables 1 and 2), shorter in **5** (M = Pd) than in **2** (M = Pt), agree with this observation.

Scheme 3

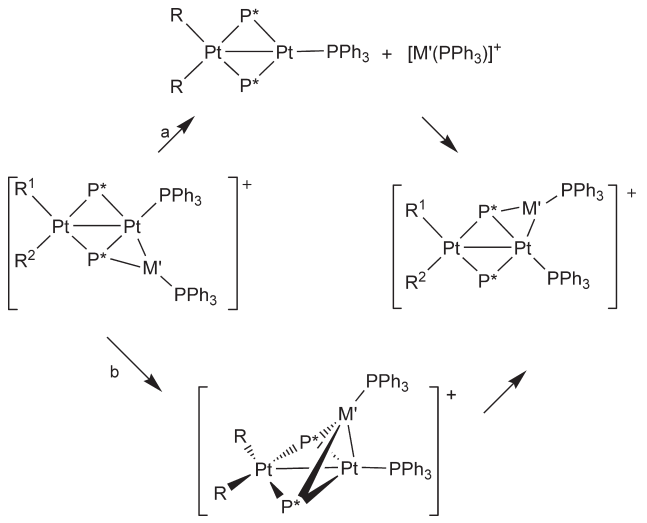

The ^{19}F NMR spectra of **2**[ClO_4], **5**[ClO_4], **6**[ClO_4], and **7**[ClO_4] ($CDCl_3$ solutions) at 213 K as well as those of **6**[ClO_4] and **7**[ClO_4] at room temperature show six signals in a 2:2:1:1:2:2 intensity ratio and indicate the inequivalence of the two C_6F_5 groups and the equivalence of both halves within each ring, in agreement with the solid-state structures. By increasing the temperature in solutions of complexes **2** and **5** (silver compounds), it can be observed that the two signals due to *o*-F atoms as well as those due to *p*-F and both signals due to *m*-F atoms collapse, and the spectra at room temperature show three broad signals in a 4:2:4 intensity ratio. This pattern confirms the presence of dynamic behavior involving the Ag(PPh_3) fragment, making both C_6F_5 groups in **2** and **5** equivalent. The Au$(PPh_3)^+$ adducts (**6** and **7**) exhibit a lower lability than those of Ag$(PPh_3)^+$, **2** and **5**.[47] Two different explanations for the equivalence of both C_6F_5 groups can be proposed. One of them involves a dissociative process (Scheme 3, path a), implying the separation of the two fragments $(C_6F_5)_2Pt(\mu\text{-}PPh_2)_2M(PPh_3)$ and M′-$(PPh_3)^+$, while the other one is an intramolecular rearrangement (Scheme 3, path b) of the $[M'(PPh_3)]^+$ fragment.

In order to discriminate between the two mechanisms (i.e., intramolecular or dissociative), we have recorded the $^{31}P\{^1H\}$ EXSY spectrum of a $CDCl_3$ solution containing **2** at 255 K (Figure 4). The presence of cross-peaks between P^1 of **2**, P^2 of **2**, and the bridging phosphide of **3** (δ 230, see inset of Figure 4)[48] demonstrates that complex **3** is involved in the exchange phenomena, thus validating the dissociative path of Scheme 1. Analogous results were obtained by $^{31}P\{^1H\}$ exchange spectroscopy

(42) Brauer, D. J.; Hessler, G.; Knuppel, P. C.; Stelzer, O. *Inorg. Chem.* **1990**, *29*, 2370–2375.
(43) Corrigan, J. F.; Doherty, S.; Taylor, N. J. *J. Am. Chem. Soc.* **1992**, *114*, 7557–7558.
(44) Leoni, P.; Pasquali, M.; Sommovigo, M.; Laschi, F.; Zanello, P.; Albinati, A.; Lianza, F.; Pregosin, P. S.; Ruegger, H. *Organometallics* **1993**, *12*, 1702–1713.
(45) Leoni, P.; Pasquali, M.; Fortunelli, A.; Germano, G.; Albinati, A. *J. Am. Chem. Soc.* **1998**, *120*, 9564–9573.
(46) Leoni, P.; Marchetti, F.; Marchetti, L.; Passarelli, V. *Chem. Commun.* **2004**, 2346–2347.
(47) Beringhelli, T.; D'Alfonso, G.; Garavaglia, M. G.; Panigati, M.; Mercandelli, P.; Sironi, A. *Organometallics* **2002**, *21*, 2705–2714.
(48) At this temperature, signals attributable to a small amount of **3** and Ag$(PPh_3)^+$ were invariably present in the $^{31}P\{^1H\}$ EXSY spectrum of **2**.

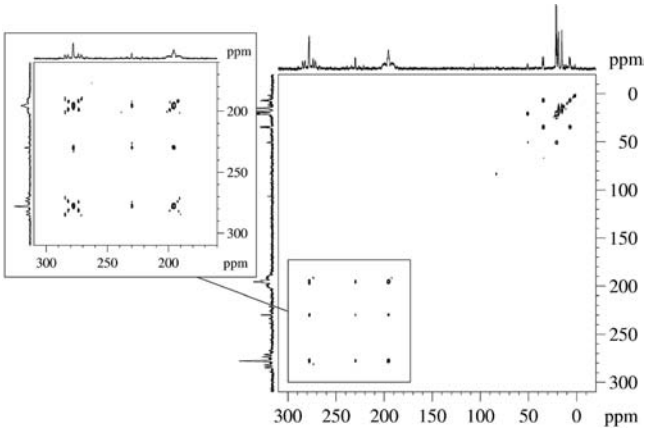

Figure 4. $^{31}P\{^{1}H\}$ EXSY spectrum of **2** ($CDCl_3$, 255 K).

(EXSY) experiments carried out on **5** at 255 K. A dissociative mechanism is also concluded from the computational study (vide infra).

As far as the gold complexes are concerned, the $^{31}P\{^{1}H\}$ EXSY of a $CDCl_3$ solution of **6** at 298 K (Figure 5) shows the exchange of the two bridging phosphido groups. The $^{31}P\{^{1}H\}$ EXSY of a $CDCl_3$ solution of a mixture of **6** and deliberately added **3**[49] (Figure 6) does not show cross-peaks between P^1 and P^2 of **6** and the P atoms of the phosphido groups of **3**. This indicates that **3** is not involved in the dynamic process of **6**, and hence an intramolecular pathway should be thought of as operative for the gold complex. This proposal is also confirmed by the $^{19}F\{^{1}H\}$ EXSY of **6** and of a mixture of **6** and **3** (Figures S2 and S3, Supporting Information).

3. Computational Study of the Reaction of 1 with Ag^+. The reaction of $[(C_6F_5)_2Pt(\mu\text{-}PPh_2)_2Pt(PPh_3)_2]$ (**1**) with Ag^+ (Scheme 2) has been computationally studied in order to clarify its mechanism. For this purpose, we have considered, as possible intermediates, the different structural isomers of the **2** cation that are shown in Scheme 4. In addition to the experimentally determined structure **2**, we have also examined the possibility of cation coordination perpendicular to the platinum coordination plane, either as $[Ag(PPh_3)]^+$ (**2A**) or Ag^+ (**2B** and **2C**). Two models were used in this study: one reduced (**r**), where all of the phenyl groups are replaced by hydrogen atoms, and one complete (**c**), where the phenyl groups were included in the geometry optimization using the quantum mechanics/molecular mechanics QM/MM methodology ONIOM[50,51] (see Computational Details section). The relative energies of all of the calculated species are shown in Table 4. Selected geometrical parameters of all of the calculated complexes are given in the Supporting Information. A comparison of the optimized geometry of cation **2** with the X-ray determined for **2[ClO4]**·$2.5CH_2Cl_2$, made in Table 1, supports the reliability of the performed BLYP/ONIOM calculations for these systems. In particular, the Pt−Ag−P bonding scheme is fairly well reproduced by calculations. The calculated Pt(1)−Ag, Ag−P(1), and Ag−P(4) bond lengths (2.763, 2.750, and 2.477 Å, respectively) differ by less than 0.1 Å from the experimental values of 2.7076, 2.686, and 2.402 Å (see Table 1).

When the relative energies of the complete model are compared with those of the reduced one, the importance of the phenyl groups in the stability of **2** can be appreciated. Thus, using the reduced model, the experimentally characterized structure **r2** is the least stable of all of them. Including solvent effects, **r2** becomes more stable than **r2A**, but the energy difference with structures bearing the Ag^+ in the plane perpendicular to the platinum coordination plane is even increased: in dichloromethane, **r2B** and **r2C** are 17.1 and 16.0 kcal mol^{-1} more stable than **r2**. Inclusion of phenyls inverts this preference, making **c2** the most stable complex. Calculation of the complete system

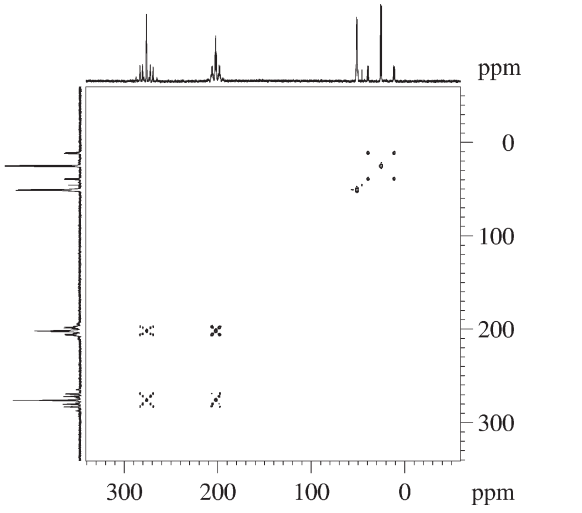

Figure 5. $^{31}P\{^{1}H\}$ EXSY spectrum of **6** ($CDCl_3$, 298 K).

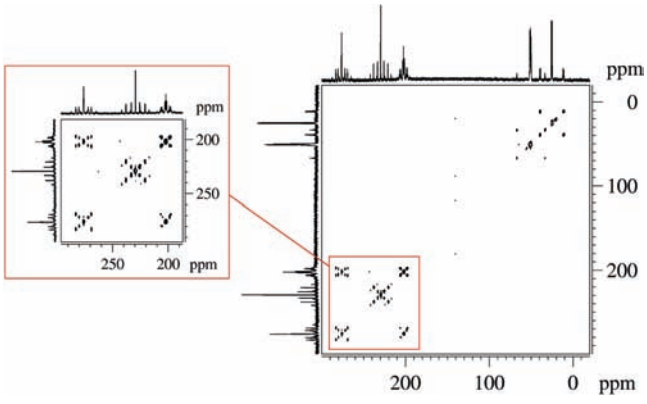

Figure 6. $^{31}P\{^{1}H\}$ EXSY spectrum of a mixture of **6** and **3** ($CDCl_3$, 298 K).

Table 4. Relative Energies (kcal·mol^{-1}) of **2**, **2A**, **2B**, and **2C** Obtained in the Gas Phase and in a Solvent (CH_2Cl_2), with a Reduced and Complete Model, Using the BLYP and BLYP/ONIOM Optimized Geometries, Respectively

	reduced (QM, gas phase)	reduced (QM, solvent)	complete (QM/MM, gas phase)	complete (QM, gas phase)	complete (QM, solvent)
2	0	0	0	0	0
2A	−3.9	4.5	0.9	2.6	7.6
2B	−9.1	−17.1	8.9	21.2	12.5
2C	−7.8	−16.0	10.9	28.0	17.6

(49) In the case of the gold cluster, no signals attributable to **3** and $Au(PPh_3)^+$ were ever detected in the $^{31}P\{^{1}H\}$ NMR spectrum of **6**.

(50) Maseras, F.; Morokuma, K. *J. Comput. Chem.* **1995**, *16*, 1170–1179.
(51) Dapprich, S.; Komaromi, I.; Byun, K. S.; Morokuma, K.; Frisch, M. J. *THEOCHEM* **1999**, *461−462*, 1.

Scheme 4. Isomers of Formula $[\{AgPt_2(\mu\text{-}PR_2)_2(C_6F_5)_2(PR_3)_2\}]$ (R = H, Ph) Considered in the Theoretical Study (P* = PR_2)

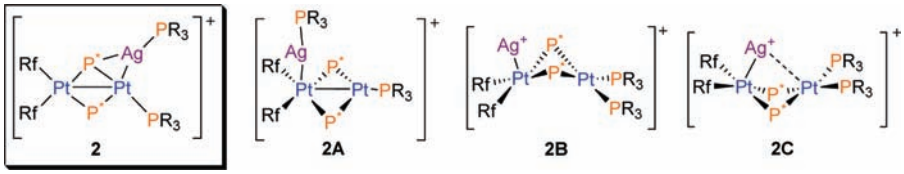

is able to reproduce the experimentally characterized structure as the most stable one. It is possible to compare QM/MM energies with the full QM energies of the reduced and complete systems in the gas phase, in order to estimate the steric and electronic contribution of the phenyl groups in the stability of these complexes (Table 4). Considering QM/MM energies and thus a purely steric effect of phenyls, **2B** and **2C**, which were the most stable isomers with the reduced model, become the less stable complexes by 10 kcal mol^{-1}. This result shows that there is an important steric effect of phenyls. To illustrate the differences between reduced and complete models, the optimized structures of the reduced **r2B** and complete **c2B** isomers are shown in Figure 7. The most important geometric change caused by Ph groups is the Pt(2) coordination geometry, which goes from an almost perfect square planar in **r2B** and **r2C** to a distorted one in **c2B** and **c2C**. This change is accompanied by an elongation of the Pt^2-P^3 and Pt^2-P^4 distances from 2.387 and 2.385 Å in **r2B** to 2.493 and 2.489 Å in **c2B**, respectively (see Figure 7). Similar changes occur in **2C**, whereas they are not observed in **2** and **2A** where P^3 and P^4 are located further away. Besides the steric effects, there is an important electronic contribution of phenyl groups, as can be seen by comparing QM/MM energies and the full QM energies using the full system. This electronic contribution and also the inclusion of a solvent act by stabilizing **c2** with respect to the other isomers **c2A**, **c2B**, and **c2C**. Calculations point to the structural preference for Ag^+ coordination in these complexes being very dependent on steric and electronic substituent effects.

On the basis of these results, the energies we report in the study of the reaction mechanism of **1** with Ag^+ are those obtained with the full QM calculations in a solvent using the complete system. Nevertheless, the model system was used to carry out some tests, for instance, Ag^+ insertion into the Pt−P bond of species such as **r2B** or **r2C**. However, no transition state could be located, and the energy increases monotonously when Ag^+ approaches the bridging phosphido group. We hence propose the stepwise process depicted in Scheme 5, which starts with the phosphine dissociation from **1** (step 1, Scheme 5). This step leads to complex **3A** with a T-shaped coordination of Pt(2). In this complex, unlike **3**, the two platinum atoms are not bonded. This can be seen by the Pt−Pt distance in **c3A** (3.641 Å) that is considerably longer than in **c3** (2.814 Å) and the angle formed by Pt(2) and the bridging phosphido groups (P1Pt2P2), which opens from 78.6° to 110.5° going from **c3A** to **c3**. This step has an energy cost of only 5.7 kcal mol^{-1}, indicating an easy phosphine dissociation in **1**. Phosphine dissociation is more difficult from complexes **c2B** and **c2C** (15.7 and 12.5 kcal mol^{-1}, respectively), showing that the first coordination of Ag^+ to Pt does not trigger the dissociation of phosphine.

Afterward, complex **3A** can rearrange to the most stable isomer **3** (step 2). In the presence of Ag^+, the free phosphine can react with Ag^+ to afford $[Ag(PPh_3)]^+$. This process is very exothermic with a reaction energy of −31.2 kcal mol^{-1} (step 3). Therefore, Ag^+ behaves as a PPh_3 scavenger, as occurs in the reaction of **1** with $[AgPPh_3]^+$ (explained above). The last step is the interaction of $[AgPPh_3]^+$ with the Pt−P bond of **3** (step 4), making the overall process thermodynamically favored by 30.7 kcal mol^{-1}.

The mechanism in Scheme 5 is consistent with the experimental observation that a dissociative path is responsible for the exchange phenomena evidenced for Ag clusters. In addition, these computational results provide a possible explanation as to why complex

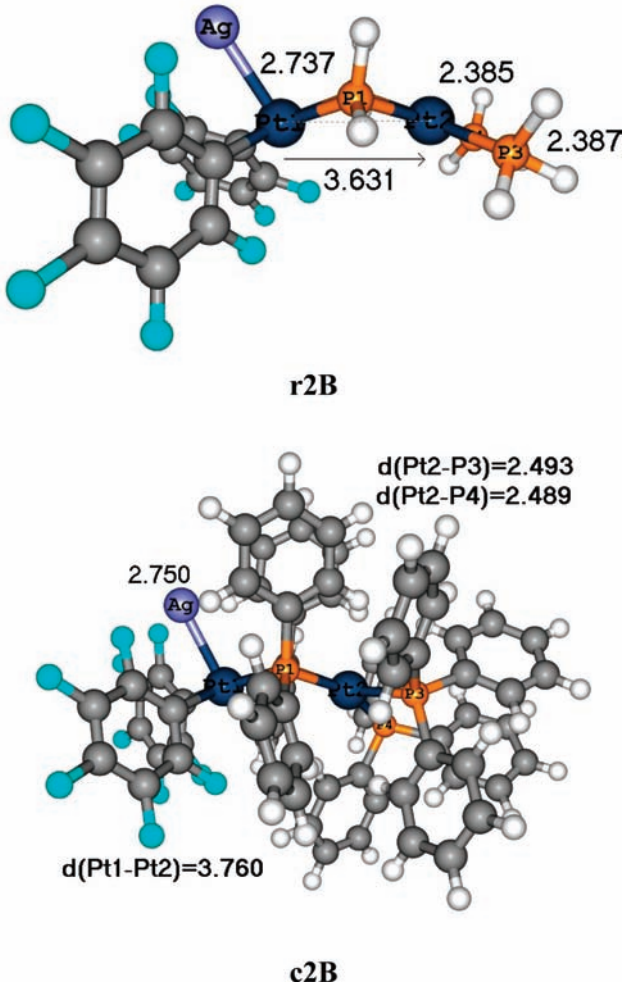

Figure 7. Optimized geometry of **2B** isomers for the reduced **r** and complete **c** model systems, with the most representative distances in ångstroms.

Scheme 5. Elementary Steps Proposed for the Reaction of $[(C_6F_5)_2Pt(\mu\text{-}PPh_2)_2Pt(PPh_3)_2]$ (**1**) with Ag^+ to Obtain $[(C_6F_5)_2Pt(\mu\text{-}PPh_2)_2Pt(PPh_3)(AgPPh_3)]^+$ (**2**)[a]

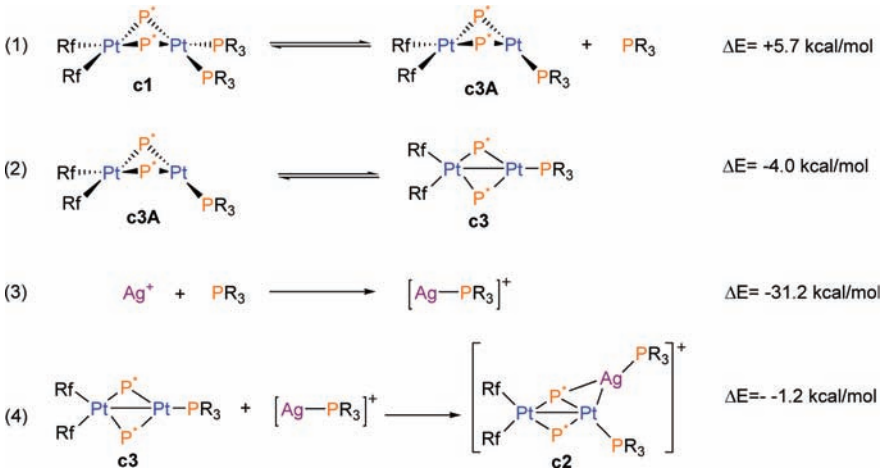

[a] Reaction energies in CH_2Cl_2 of each step are also included.

$[(C_6F_5)_2Pt(\mu\text{-}PPh_2)_2Pt(L)_2]$ yields **2** with L = PPh_3, while with $(L)_2$ = acac, the same reaction yields the analogous **2C** isomer (see Scheme 1b). First, the analysis of **2** isomers has shown that the steric effects of Ph groups stabilize **2** in front of **2C**. Second, the formation of product **2** requires the dissociation of one L ligand, this step being much easier with neutral monodentate ligands than with anionic chelate ligands. If there is no decoordination of L in **1**, Ag^+ can only coordinate Pt out of the plane formed by the other ligands.

4. Analysis of (R_2P−Pt)−Ag Interaction. The behavior of **3** and **4** toward the silver or gold fragment "$M'(PPh_3)^+$" is noteworthy. In fact, it has already been reported that complexes **3** and **4** react with neutral or anionic ligands, giving rise to the 32-VEC complexes $[(C_6F_5)_2Pt(\mu\text{-}PPh_2)_2M(PPh_3)L]^{n-}$ (M = Pd, Pt; n = 1, 0), which do not require a Pt−M bond, in a process in which the M center of **3** or **4** acts as a Lewis acid toward the incoming ligand L.[23] However, the formation of cations **2** and **5**−**7** indicates that the M−P(phosphido) bond behaves as a Lewis base toward the "$Ag(PPh_3)^+$"or "$Au(PPh_3)^+$" fragments. In this case, the silver or gold center could be neutralized by the Ph_2P−M (M = Pt, Pd) bond, giving rise to a three-center−two-electron system Ph_2P−Ag−M(II) or Ph_2P−Au−M(II). This interpretation is in agreement with the molecular orbital and natural bond orbital (NBO) analysis performed for **r2** and **r3**. The electronic structure analysis of **r3** shows a doubly occupied π orbital close to the frontier level (HOMO−5, see Figure 8a). The shape and symmetry of this orbital suggest that **r3** may act as a Lewis base coordinating to $[Ag(PPh_3)]^+$ on the Ph_2P−Pt plane. In addition, the NBO analysis performed for **r2** shows that the natural localized molecular orbital (NLMO) for the Ph_2P−Ag−Pt(II) bond has an important contribution from Ag, P^1, and Pt^1 (χ^{Ag} = 15.36%, χ^{P} = 66.30%, and χ^{Pt} = 9.56%), displaying a three-center, two-electron nature (see Figure 8b). The elongation of the P^1−Pt^1 bond in going from **r3** (2.333 Å) to **r2** (2.389 Å) also indicates that the electrons participating in this interaction come from the P^1−Pt^1 bond. This elongation becomes higher for the complete system, from 2.314 Å in **c3** to 2.413 Å in **c2**. This three-center interaction is expected to be weak considering the small binding energy of $[AgPPh_3]^+$ to **c3** (−1.2 kcal mol^{-1}, Scheme 5, step 4). An estimation of the strength of Ag−P^1 and Ag−Pt^1 interactions can be made by calculating the energy required to elongate these bonds in **r2**. For this purpose, one-dimensional potential energy curves have been computed starting from the optimized structure of **r2** and increasing the Ag−P^1 and Ag−Pt^1 distances, optimizing the rest of the geometric parameters for each fixed value of these distances. These calculations show that, if the Ag−P^1 distance is lengthened from 2.773 Å (distance in **r2**) to 3.200 Å, the energy only increases 1.9 kcal mol^{-1}, while elongation of the Ag−Pt^1 bond from 2.793 Å (distance in r2) to 3.200 Å, increases the energy 3.6 kcal mol^{-1}. In both cases, the ΔE values are very low, proving that bonding of $[AgPPh_3]^+$ to $[(C_6F_5)_2Pt(\mu\text{-}PPh_2)_2Pt(PPh_3)]$ results from the addition of two weak interactions. The coordination of both fragments in cations **2** and **5**−**7** implies that the P atom of the phosphido group is bridging three metal centers. Such a μ_3-bonding mode for the μ-PR_2 ligand is not the typical coordination mode for a phosphido ligand, although complexes in which this phosphorus center shows five coordination are known,[28,33−36,42,43,52−60] as are bridging phosphine ligands.[61−63]

Cations **2** and **5**−**7** can also be related with the unusual tetranuclear Pt−Au cluster $[\{AuPt(\mu\text{-}PPh_2)(PPh_3)_2\}_2]^{2+}$,[28]

(52) Jones, R. A.; Stuart, A. L.; Wright, T. C. *J. Am. Chem. Soc.* **1983**, *105*, 7459–7460.
(53) Driess, M.; Huttner, G.; Knopf, N.; Pritzkow, H.; Zsolnai, L. *Angew. Chem., Int. Ed. Engl.* **1995**, *34*, 316–318.
(54) Hey-Hawkins, E.; Sattler, E. *J. Chem. Soc., Chem. Commun.* **1992**, 775–776.
(55) Englich, U.; Hassler, K.; Ruhlandt-Senge, K.; Unlig, F. *Inorg. Chem.* **1998**, *37*, 3532–3537.
(56) Hey, E.; Hitchcock, P. B.; Lappert, M. F.; Rai, A. K. *J. Organomet. Chem.* **1987**, *325*, 1–12.
(57) Eichhofer, A.; Fenske, D.; Holstein, W. *Angew. Chem., Int. Ed. Engl.* **1993**, *32*, 242–245.
(58) Knoll, K.; Huttner, G.; Wasiucioneck, M.; Zsolnai, L. *Angew. Chem., Int. Ed. Engl.* **1984**, *23*, 739–740.
(59) Gol, F.; Knuppel, P. C.; Stelzer, O.; Sheldrick, W. S. *Angew. Chem., Int. Ed. Engl.* **1988**, *27*, 956–957.
(60) Chaouche, N.; Forniés, J.; Fortuño, C.; Kribii, A.; Martín, A. *J. Organomet. Chem.* **2007**, *692*, 1168–1172.
(61) Pechmann, T.; Brandt, C. D.; Werner, H. *Dalton Trans.* **2004**, 959–966.
(62) Leca, F.; Sauthier, M.; Deborde, V.; Toupet, L.; Réau, R. *Chem. Eur. J.* **2003**, *9*, 3785–3795.
(63) Braunstein, P.; Boag, N. M. *Angew. Chem., Int. Ed. Engl.* **2001**, *40*, 2427–2433.

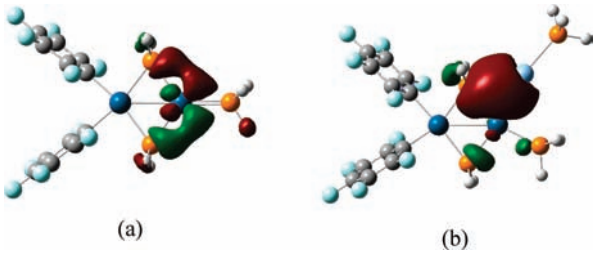

Figure 8. (a) Graphical representation of the HOMO−5 in **r3** and (b) the NLMO corresponding to the P−Ag−Pt interaction in **r2** from a NBO analysis.

reported by Braunstein and co-workers and resulting from formal addition of the electrophile "$Au(PPh_3)^+$" to two Pt−(μ-P) bonds of the dinuclear Pt(I) derivative [{Pt(μ-PPh_2)(PPh_3)}$_2$], while the isolobal electrophilic group "Ag-$(PPh_3)^+$" does not give a stable, isolable complex.[7] Leoni and co-workers have observed related behavior in the reaction processes of the M(I) derivatives [M_2(μ-P^{t}Bu$_2$)$_2$-(P^{t}Bu$_2$H)$_2$] (M = Pd, Pt) with H^+. For M = Pd, the complex [Pd_2(μ-P^{t}Bu$_2$)(μ-P^{t}Bu$_2$H)(P^{t}Bu$_2$H)$_2$]$^+$ was obtained, in which the new phosphine ligand is bridging two palladium centers, giving rise to a three-center P−H−Pd bond.[44] Nevertheless, for M = Pt, the derivative [Pt_2(μ-P^{t}Bu$_2$)$_2$(H)(P^{t}Bu$_2$H)$_2$]$^+$, in which the incoming H^+ is substantially bonded to the platinum center as a terminal hydride, was obtained.[45,64] A rare (μ-P)−H−Pt system has been observed as a consequence of the protonation of [Pt_2(μ-P^{t}Bu$_2$)$_2$(η^2-CH_2=CH_2)$_2$].[46] As far as we know, the coordination of the (μ-P)−M(II) (M = Pt, Pd) bonds to a silver center to give the 3c−2e P−Ag−M(II) bonds present in cations **2** and **5** is unprecedented.

Concluding Remarks

The behavior of complexes [$(C_6F_5)_2$Pt(μ-PPh_2)$_2$PtL_2]$^{n-}$ (L = C_6F_5, n = 2; L_2 = acac, n = 1; L = PPh_3 n = 0) toward silver centers is highly dependent on L. For L = PPh_3, the Ag^+ ion inserts into the Pt−PPh_3 bond, giving rise, to the best of our knowledge, to the first 2e−3c (μ-PPh_2)−Ag−Pt(II) system. The structure of cations **2** and **5**−**7** exhibits a PPh_2 group in a nonclassical coordination mode, that is, as a bridging ligand between three metal centers. Analysis of the electronic structure of **2** indicates that the formation of **2**, **5**, and **7** from **3** or **4** and [M′PPh_3]$^+$ (M′ = Ag, Au) can be interpreted as the result of the interaction between the M−PPh_2 (M = Pt, Pd) bond of **3** and **4** and [M′PPh_3]$^+$ (M′ = Ag, Au). The NLMO representing this interaction in **2**, corresponding to a Ag−P (phosphide) bond orbital, has an important contribution of Ag, P and Pt, thus showing a three-center−two-electron nature. The bonding between the two moieties results from the addition of two weak interactions: Ag−P (phosphide) and Ag−Pt. The synthesis of these four complexes from the dinuclear **3** and **4** proves the capability of a P−M(II) (M = Pt, Pd) bond in a "classical" phosphido bridging ligand to act as a donor toward M′PPh_3^+ (M′ = Ag, Au), resulting in a best described P−M′−M(II) multicentered interaction (3c−2e, as confirmed by NBO analysis), which is maintained in solution. In summary, the M−(μ-P) bond of complexes [$(C_6F_5)_2$Pt(μ-PPh_2)$_2$M(PPh_3)] (M = Pt, Pd) is more electron rich than the platinum and palladium centers.

The computational study of the reactivity of **1** with $[Ag]^+$ explains the experimental findings by a mechanism which involves the following steps: (1) decoordination of one PPh_3 ligand, resulting in a T-shaped tricoordinate Pt (structure **3A**), (2) rearrangement of **3A** to give **3** with a trigonal Pt and a Pt−Pt bond, (3) bonding of the decoordinated PPh_3 and Ag^+ with the formation of [$AgPPh_3$]$^+$, and (4) interaction of this cation with the Pt−PPh_3 bond of **3**. The slight difference in energy between **2** and **3** + [$AgPPh_3$]$^+$ (ΔE = 1.2 kcal mol^{-1}) suggests an equilibrium of these two complexes in solution (apparent from multinuclear EXSY experiments), which allows a facile change in the position of [$AgPPh_3$]$^+$. In addition, the analysis of the [$(C_6F_5)_2Pt_2$(μ-PPh_2)$_2$(PPh_3)$_2$Ag] isomers shows an important effect of the Ph substituents in the stabilization of structure **2**. The presence of phenyl groups favors, by both steric and electronic effects, the formation of isomer **2**, with Ag^+ in the platinum coordination plane, over **2B** or **2C**, with Ag^+ perpendicular to the platinum coordination plane.

Experimental Section

General Comments. Literature methods were used to prepare the starting materials [$(C_6F_5)_2$Pt(μ-PPh_2)$_2$Pt(PPh_3)$_2$],[21] [$(C_6F_5)_2$-Pt(μ-PPh_2)$_2$M(PPh_3)] (M = Pt, Pd),[23] [Ag($OClO_3$)PPh_3],[65] and [AuCl(PPh_3)].[66] C and H analysis and IR and NMR spectra were performed as described elsewhere.[67]

Caution! *Perchlorate salts of metal complexes with organic ligands are potentially explosive. Only small amounts of materials should be prepared, and these should be handled with great caution.*

Synthesis of [AgMPt(μ-PPh_2)$_2$(C_6F_5)$_2$(PPh_3)$_2$][ClO_4] (M = Pt, 2[ClO_4]; Pd, 5[ClO_4]). M = Pt, 2[ClO_4]. a. To a yellow solution of [$(C_6F_5)_2$Pt(μ-PPh_2)$_2$Pt(PPh_3)$_2$] (0.100 g, 0.062 mmol) in CH_2Cl_2 (30 mL) was added $AgClO_4$ (0.014 g, 0.067 mmol), and the mixture was stirred at room temperature for 2 h. After filtration, the resulting orange solution was evaporated to ca. 1 mL. The addition of *n*-hexane (10 mL) caused the precipitation of an orange solid, **2[ClO_4]**, which was filtered off and washed with *n*-hexane (3 × 1 mL), 0.080 g, 71% yield.

b. To a red solution of **3** (0.200 g, 0.149 mmol) in CH_2Cl_2 (10 mL) was added [Ag($OClO_3$)PPh_3] (0.070 g, 0.147 mmol), and the orange solution was stirred for 5 min and then evaporated to ca. 1 mL. The addition of *n*-hexane (10 mL) caused the precipitation of **2[ClO_4]**, which was filtered off and washed with *n*-hexane (3 × 1 mL), 0.254 g, 94% yield. Anal. Found (Calcd) for $AgC_{72}ClF_{10}H_{50}O_4P_4Pt_2$: C, 47.0 (47.3); H, 2.5 (2.8). IR (cm^{-1}): 781, 793 (X-sensitive, C_6F_5).[68,69] ^{19}F NMR ($CDCl_3$, 213 K, 282.4 MHz): δ −119.3 (2 *o*-F, $^3J_{Pt,F}$ = 301 Hz), −119.8 (2 *o*-F, $^3J_{Pt,F}$ = 334 Hz), −158.4 (1 *p*-F), −158.7 (1 *p*-F), −162.1 (2 *m*-F), −162.5 (2 *m*-F). $^{31}P\{^1H\}$ NMR ($CDCl_3$, 213 K, 161.9 MHz): δ 277.7 (P^2, $^1J_{Pt^5,P^2}$ = 1386, $^1J_{Pt^6,P^2}$ = 2135 Hz), 195.8 (P^1, $^1J_{P^1,^{109/107}Ag} \approx 140$ Hz, $^2J_{P^1,P^4}$ = 37 Hz), 19.8 (P^3, $^2J_{P^3,P^1}$ = 153, $^2J_{P^3,P^2}$ = 8, $^1J_{Pt^6,P^3}$ = 4497, $^2J_{Pt^5,P^3}$ = 81 Hz), 15.8 (P^4, $^1J_{P^4,^{109}Ag} \approx 580$ Hz, $^1J_{P^4,^{107}Ag} \approx 505$ Hz, $^2J_{P^4,P^1}$ = 37, $^3J_{P^4,P^2}$ = 24) ppm.

M = Pd, 5[ClO_4]. Complex **5[ClO_4]** was prepared at 273 K similarly from **4** (0.075 g, 0.059 mmol) and [Ag($OClO_3$)PPh_3]

(64) Albinati, A.; Leoni, P.; Marchetti, F.; Marchetti, L.; Pasquali, M.; Rizzato, S. *Eur. J. Inorg. Chem.* **2008**, 4092–4100.

(65) Cotton, F. A.; Falvello, L. R.; Usón, R.; Forniés, J.; Tomás, M.; Casas, J. M.; Ara, I. *Inorg. Chem.* **1987**, *26*, 1366–1370.

(66) Usón, R.; Laguna, A. *Inorg. Synth.* **1982**, *21*, 71–74.

(67) Ara, I.; Forniés, J.; Fortuño, C.; Ibáñez, S.; Martín, A.; Mastrorilli, P.; Gallo, V. *Inorg. Chem.* **2008**, *47*, 9069–9080.

(68) Usón, R.; Forniés, J. *Adv. Organomet. Chem.* **1988**, *28*, 219–297.

(69) Maslowsky, E. J. *Vibrational Spectra of Organometallic Compounds*; Wiley: New York, 1997.

Table 5. Crystal Data and Structure Refinement for $[AgPt_2(\mu\text{-}PPh_2)_2(C_6F_5)_2(PPh_3)_2][ClO_4]\cdot 2.5CH_2Cl_2$ (**2[ClO$_4$]**·2.5CH_2Cl_2), $[AgPtPd(\mu\text{-}PPh_2)_2(C_6F_5)_2(PPh_3)_2][ClO_4]\cdot 4CH_2Cl_2$ (**5[ClO$_4$]**·4CH_2Cl_2), and $[AuPt_2(\mu\text{-}PPh_2)_2(C_6F_5)_2(PPh_3)_2][ClO_4]\cdot 2.5CH_2Cl_2$ (**6[ClO$_4$]**·2.5CH_2Cl_2)

complex	**2[ClO$_4$]**·2.5CH_2Cl_2	**5[ClO$_4$]**·4CH_2Cl_2	**6[ClO$_4$]**·2.5CH_2Cl_2
empirical formula	$C_{72}H_{50}ClF_{10}O_4AgP_4Pt_2\cdot 2.5CH_2Cl_2$	$C_{72}H_{50}ClF_{10}O_4P_4AgPdPt\cdot 4CH_2Cl_2$	$C_{72}H_{50}ClF_{10}O_4AuP_4Pt_2\cdot 2.5CH_2Cl_2$
unit cell dimensions			
a (Å)	12.7400(10)	13.4884(6)	12.6684(7)
b (Å)	13.8405(20)	13.9324(7)	13.7285(8)
c (Å)	23.1136(32)	21.5019(10)	23.0192(13)
α (deg)	90.734(7)	91.690(1)	90.879(1)
β (deg)	91.811(6)	99.239(1)	91.976(1)
γ (deg)	113.422(7)	99.983(1)	113.606(1)
V (Å^3), Z	3736.5(8), 2	3921.1(3), 2	3664.4(4), 2
wavelength (Å)	0.71073	0.71073	0.71073
temp (K)	173(1)	100(1)	100(1)
radiation	graphite monochromated Mo Kα	graphite monochromated Mo Kα	graphite monochromated Mo Kα
cryst syst	triclinic	triclinic	triclinic
space group	$P\bar{1}$	$P\bar{1}$	$P\bar{1}$
cryst dimensions (mm)	0.45 × 0.30 × 0.25	0.49 × 0.29 × 0.19	0.49 × 0.47 × 0.40
abs coeff (mm^{-1})	4.368	2.714	6.186
abs corrn	4063 symmetry equivalent reflns	SADABS[71]	SADABS[71]
diffractometer	Siemens SMART	Bruker SMART	Bruker SMART
2θ range for data collect. (deg)	3.20−52.22	3.12−50.06	3.24−50.06
no. of rflns collected	18383	21614	20227
no. of independent rflns	12478 [R(int) = 0.0708]	13616 [R(int) = 0.0234]	12733 [R(int) = 0.0143]
refinement method	full-matrix least-squares on F^2	full-matrix least-squares on F^2	full-matrix least-squares on F^2
goodness-of-fit on F^2[a]	1.129	1.034	1.023
final R indices ($I > 2\sigma(I)$)[b]	R1 = 0.0589, wR2 = 0.1474	R1 = 0.0395 wR2 = 0.0926	R1 = 0.0225 wR2 = 0.0551
R indices (all data)	R1 = 0.0663, wR2 = 0.1564	R1 = 0.046 wR2 = 0.0952	R1 = 0.0259 wR2 = 0.0560

[a] Goodness-of-fit = $[\sum w(F_o^2 - Fc^2)^2 / (n_{obs} - n_{param})]^{1/2}$. [b] $R_1 = \sum(|F_o| - |F_c|)/\sum |F_o|$. $wR_2 = [\sum w(F_o^2 - Fc^2)^2/\sum w(F_o^2)^2]^{1/2}$.

(0.027 g, 0.057 mmol) as an orange solid. **5[ClO$_4$]**: 0.070 g, 68% yield. Anal. Found (Calcd) for $AgC_{72}ClF_{10}H_{50}O_4P_4PdPt$: C, 49.5 (49.8); H, 3.2 (2.9). IR (cm^{-1}): 781, 792 (X-sensitive, C_6F_5). ^{19}F NMR ($CDCl_3$, 213 K, 282.4 MHz): δ −119.2 (2 *o*-F, $^3J_{Pt,F}$ = 301 Hz), −119.8 (2 *o*-F, $^3J_{Pt,F}$ = 311 Hz), −158.4 (1 *p*-F), −159.2 (1 *p*-F), −162.2 (2 *m*-F), −162.5 (2 *m*-F). $^{31}P\{^1H\}$ NMR ($CDCl_3$, 213 K, 121.4 MHz): δ 305.3 (P^2, $^1J_{Pt^5,P^2}$ = 1555 Hz), 174.9 (P^1, $^1J_{Pt^5,P^1} \approx 1200$ Hz), 25.1 (P^3, $^2J_{P^3,P^1}$ = 106 Hz, $^2J_{P^3,P^2}$ = 11 Hz, $^2J_{Pt^5,P^3}$ = 101 Hz), 15.1 (P^4, $^1J_{P^4,^{109}Ag} \approx 575$ Hz, $^1J_{P^4,^{107}Ag} \approx 500$ Hz) ppm.

Synthesis of [AuMPt(μ-PPh$_2$)$_2$(C$_6$F$_5$)$_2$(PPh$_3$)$_2$][ClO$_4$] (M = Pt, 6[ClO$_4$]; Pd, 7[ClO$_4$]). M = Pt, 6[ClO$_4$]. A mixture of $AgClO_4$ (0.036 g, 0.174 mmol) and [AuCl(PPh$_3$)] (0.076 g, 0.154 mmol) in CH_2Cl_2 (25 mL) was stirred at 273 K in the dark for 1 h. The mixture was filtered through Celite, and **3** (0.200 g, 0.147 mmol) was added to the colorless filtrate at 273 K. The orange solution was stirred for 5 min, evaporated to 3 mL, and *n*-hexane (15 mL) added, giving rise to orange oil. *n*-Hexane (10 mL) was added to the oil, and after stirring, an orange solid, **6[ClO$_4$]**, was formed, which was filtered and washed with 3 × 1 mL of *n*-hexane, 0.170 g, 60%. Anal. Found (Calcd) for $AuC_{72}ClF_{10}H_{50}O_4P_4Pt_2$: C, 45.1 (45.6); H, 2.6 (2.6). IR (cm^{-1}): 780, 792 (X-sensitive, C_6F_5).[68,69] ^{19}F NMR ($CDCl_3$, 295 K, 282.4 MHz): δ −118.4 (2 *o*-F, $^3J_{Pt,F}$ = 282 Hz), −119.2 (2 *o*-F, $^3J_{Pt,F}$ = 339 Hz), −159.2 (1 *p*-F), −159.5 (1 *p*-F), −162.4 (2 *m*-F), −162.9 (2 *m*-F). $^{31}P\{^1H\}$ NMR ($CDCl_3$, 295 K, 121.4 MHz): δ 276.0 (P^2, $^1J_{Pt^5,P^2}$ = 1356, $^1J_{Pt^6,P^2}$ = 2255 Hz), 202.0 (P^1, $^2J_{P^1,P^2}$ = 58, $^2J_{P^1,P^4}$ = 90, $^2J_{P^1,P^3}$ = 165, $^1J_{Pt^{5or6},P^1}$ = 1102 and 1411 Hz), 50.9 (P^4, $^2J_{P^2,P^4}$ = 45, $^2J_{P^1,P^4}$ = 90, $^2J_{Pt^6,P^4}$ = 257), 25.1 (P^3, $^2J_{P^1,P^3}$ = 165, $^1J_{Pt^6,P^3}$ = 4508, $^2J_{Pt^5,P^3}$ = 81 Hz) ppm.

M = Pd, 7[ClO$_4$]. This complex was prepared by the same procedure as that used for **6[ClO$_4$]**, from 0.025 g (0.120 mmol) of $AgClO_4$, 0.058 g (0.117 mmol) of [AuCl(PPh$_3$)], and 0.147 g (116 mmol) of **4**, and was yielded as an orange solid, **7[ClO$_4$]**, 0.145 g, 68%. Anal. Found (Calcd) for $AuC_{72}ClF_{10}H_{50}O_4P_4PdPt$: C, 47.43 (47.33); H, 2.84 (2.76). IR (cm^{-1}): 782, 794 (X-sensitive, C_6F_5).[68,69] ^{19}F NMR ($CDCl_3$, 295 K, 282.4 MHz): δ −118.2 (2 *o*-F, $^3J_{Pt,F}$ = 286 Hz), −119.3 (2 *o*-F, $^3J_{Pt,F}$ = 304 Hz), −159.0 (1 *p*-F), −160.1 (1 *p*-F), −162.4 (2 *m*-F), −162.8 (2 *m*-F). $^{31}P\{^1H\}$ NMR ($CDCl_3$, 295 K, 121.4 MHz): δ 301.8 (P^2, $^1J_{Pt^5,P^2}$ = 1594 Hz), 165.5 (P^1, $^2J_{P^1,P^2}$ = 40, $^2J_{P^1,P^3}$ = 108, $^2J_{P^1,P^4}$ = 138, $^1J_{Pt^5,P^1}$ = 1244 Hz), 50.6 (P^4, $^3J_{P^3,P^4}$ = 18, $^2J_{P^2,P^4}$ = 35, $^2J_{P^1,P^4}$ = 138, $^3J_{Pt^5,P^4}$ = 56), 32.6 (P^3, $^2J_{P^1,P^3}$ = 108, $^3J_{P^3,P^4} \approx {}^2J_{P^2,P^3} \approx$ 18, $^2J_{Pt^5,P^3}$ = 95 Hz) ppm.

X-Ray Structure Determination. Crystal data and other details of the structure analysis are presented in Table 5. Suitable crystals of **2[ClO$_4$]**·2.5CH_2Cl_2, **5[ClO$_4$]**·4CH_2Cl_2, and **6[ClO$_4$]**·2.5CH_2Cl_2 were obtained by slow diffusion of *n*-hexane into a CH_2Cl_2 solution of the complex. Crystals were mounted at the end of a glass fiber. For **2[ClO$_4$]**·2.5CH_2Cl_2, unit cell dimensions were initially determined from the positions of 408 reflections in 90 intensity frames measured at 0.3° intervals in ω and subsequently refined on the basis of positions of 6552 reflections from the main data set. An absorption correction was applied on the basis of 952 symmetry-equivalent reflection intensities. For **5[ClO$_4$]**·4CH_2Cl_2, unit cell dimensions were initially determined from the positions of 212 reflections in 60 intensity frames measured at 0.3° intervals in ω and subsequently refined on the basis of positions of 952 reflections from the main data set. For **6[ClO$_4$]**·2.5CH_2Cl_2, unit cell dimensions were initially determined from the positions of 275 reflections in 90 intensity frames measured at 0.3° intervals in ω and subsequently refined on the basis of positions of 6981 reflections from the main data set. The diffraction frames were integrated using the SAINT package[70] and corrected for absorption with SADABS[71] for **5[ClO$_4$]**·4CH_2Cl_2 and **6[ClO$_4$]**·2.5CH_2Cl_2, and on the basis of 952 symmetry equivalent reflection intensities for 2[ClO_4]·2.5CH_2Cl_2. Lorentz and polarization corrections were applied for the three structures.

The structures were solved by Patterson and Fourier methods. All refinements were carried out using the program SHELXL-97.[72] All non-hydrogen atoms were assigned anisotropic displacement

(70) *SAINT-Plus*, version 6.02; Bruker Analytical X-ray Systems, Inc.: Madison, WI, 1999.

(71) Sheldrick, G. M. *SADABS*; University of Gottingen: Gottingen, Germany, 1996.

(72) Sheldrick, G. M. *SHELXL-97*; University of Gottingen: Gottingen, Germany, 1997.

parameters and refined without positional constraints, except as noted below. All hydrogen atoms were constrained to idealized geometries and assigned isotropic displacement parameters 1.2 times the U_{iso} value of their attached carbon atoms (1.5 times for methyl hydrogen atoms). For **2[ClO$_4$]**·2.5CH_2Cl_2, constraints in the C−Cl distances were applied for the half-occupancy dichloromethane solvent molecule. For **5[ClO$_4$]**·4CH_2Cl_2, of the four CH_2Cl_2 solvent molecules, two were disordered, one over two sets of positions refined with 0.50/0.50 occupancy and the other over three positions refined with occupancy 0.33/0.33/0.33. For these disordered moieties, constraints in their interatomic distances were applied. For **6[ClO$_4$]**·2.5CH_2Cl_2, half of a molecule of dichloromethane solvent was found near an inversion center and its C and H atoms refined with a partial occupancy of 0.5. The interatomic distances for this molecule were constrained to sensible values. Full-matrix least-squares refinement of these models against F^2 converged to final residual indices given in Table 5. For **2-[ClO$_4$]**·2.5CH_2Cl_2, final difference electron density maps showed 41 peaks above 1 e Å^{-3} (max and min electron density 2.97 and −2.90 e Å^{-3}), the biggest of which lie close to the heavy and solvent atoms. These features are consistent with the presence of systematic errors in the intensity data. Variations in the integration procedures (changing integration "shoebox" sizes etc.) and in the absorption correction methods did not improve the Rint or final wR_2 values or reduce the size of features in the final difference map. In addition, the molecular geometry determined remained essentially invariant throughout. For **5[ClO$_4$]**·4CH_2Cl_2, final difference electron density maps showed five peaks above 1 e Å^{-3} (max/min, +1.34/−1.90) very close to the Cl atoms of the disordered molecules or the Pt atom. For **2[ClO$_4$]**·2.5CH_2Cl_2, final difference electron density maps showed two peaks above 1 e Å^{-3} (1.96, 1.76; largest diff. hole, −1.84), all of them in close vicinity of the disordered solvent.

Computational Details. This study has been performed using two different models: the reduced (**r**) model, in which all of the phenyls have been replaced by H, and the complete (**c**) model, in which the full system has been considered. All calculations were performed using the Gaussian 03 package.[73] The geometries of the minima with the reduced model were fully optimized using density functional theory with the BLYP functional,[74,75] which has been shown to correctly reproduce the bond energy and geometries of M−M interactions.[76] To check the consistency of the BLYP energies, additional single-point MP2 calculations were carried out at the BLYP optimized structures. No significant changes in the relative stabilities of the different isomers were found (see the Supporting Information). Geometry optimizations with the complete systems were carried out using the ONIOM method.[50,51] This hybrid QM/MM method was applied, dividing the system into two parts. One of these parts was computed at the quantum mechanical level (QM part) using the BLYP functional,[74,75] and the other was computed with a molecular mechanics method (MM part) using the UFF force field.[77] The particular QM/MM partition adopted in this study includes the full reduced system in the QM part and the phenyl groups in the MM part. Single-point full QM calculations of the complete systems were also performed at the optimized ONIOM geometries using the BLYP functional. To check the consistency of the BLYP energies, additional single-point MP2 calculations were carried out at the BLYP optimized structures of the reduced model. No significant changes in the relative stabilities of the different isomers were found (see Table S1 in the Supporting Information). In addition, single-point-energy-only LMP2[78,79] and M06[80] calculations were performed at the BLYP/ONIOM optimized geometries of the complete systems (**c2**, **c2A**, **c2B**, and **c2C**) to estimate the importance of noncovalent interactions in discriminating between these isomers. These interactions stabilize more the **c2B** and **c2C** isomers than the **c2** and **c2A** ones, **c2** and **c2B** being almost isoenergetic at both the LMP2 and M06 computational levels (see Table S2 in the Supporting Information for details). However, as discussed above, phosphine dissociation from **c2B** is more difficult than from **1**, and thus the conclusions about the mechanism proposed in Scheme 5 remain unchanged. Test calculations with the LMP2 methodology and with the M06 functional were carried out with the Jaguar V7.0 program.[81]

In the QM calculations with the Gaussian 03 package,[73] the lanl2dz effective core potential has been used to describe the inner electrons for the Pt, Ag, and P atoms,[82] whereas their associated double-ζ basis set has been employed for the remaining electrons. An extra series of d-polarization functions has also been added in P atoms (exp. 0.387) and f functions in Pt and Ag atoms (exp. 0.993 and 1.611, respectively).[83,84] The carbon and fluorine atoms have been described by the 6-31G(d,p) basis set and hydrogen atoms by the 6-31G basis set.[85,86] The structures of the reactants, intermediates, and products were fully optimized without any symmetry restriction. Single-point solvent calculations were performed at the optimized gas-phase geometries, using the conductor polarized continuum model approach,[87,88] which is an implementation of the conductor-like screening solvation model in Gaussian 03.[89] Dichloromethane, the solvent used in experiments, was chosen (dielectric constant $\varepsilon = 8.93$). The electronic structure of **2** was analyzed through NBO analysis, in which NLMOs were computed.[90,91]

In the single-point QM calculations with Jaguar V7.0,[81] the LACV3P basis set has been used[92] to describe Pt and Ag, and the LAV3P for the P atoms. The carbon and fluorine atoms have

(73) Frisch, M. J.; Trucks, G. W.; Schlegel, H. B.; Scuseria, G. E.; Robb, M. A.; Cheeseman, J. R.; Montgomery, J. A. J.; Vreven, T.; Kudin, K. N.; Burant, J. C.; Millam, J. M.; Iyengar, S. S.; Tomasi, J.; Barone, V.; Mennucci, B.; Cossi, M.; Scalmani, G.; Rega, N.; Petersson, G. A.; Nakatsuji, H.; Hada, M.; Ehara, M.; Toyota, K.; Fukuda, R.; Hasegawa, J.; Ishida, M.; Nakajima, T.; Honda, Y.; Kitao, O.; Nakai, H.; Klene, M.; Li, X.; Knox, J. E.; Hratchian, H. P.; Cross, J. B.; Adamo, C.; Jaramillo, J.; Gomperts, R.; Stratmann, R. E.; Yazyev, O.; Austin, A. J.; Cammi, R.; Pomelli, C.; Ochterski, J. W.; Ayala, P. Y.; Morokuma, K.; Voth, G. A.; Salvador, P.; Dannenberg, J. J.; Zakrzewski, V. G.; Dapprich, S.; Daniels, A. D.; Strain, M. C.; Farkas, O.; Malick, D. K.; Rabuck, A. D.; Raghavachari, K.; Foresman, J. B.; Ortiz, J. V.; Cui, Q.; Baboul, A. G.; Clifford, S.; Cioslowski, J.; Stefanov, B. B.; Liu, G.; Liashenko, A.; Piskorz, P.; Komaromi, I.; Martin, R. L.; Fox, D. J.; Keith, T.; Al-Laham, M. A.; Peng, C. Y.; Nanayakkara, A.; Challacombe, M.; Gill, P. M. W.; Johnson, B.; Chen, W.; Wong, M. W.; Gonzalez, C.; Pople, J. A.; *Gaussian 03*, revision C.02; Gaussian, Inc.: Wallingford CT, 2004.
(74) Becke, A. D. *Phys. Rev. A* **1988**, *38*, 3098–3100.
(75) Lee, C.; Parr, R. G.; Yang, W. *Phys. Rev. B* **1988**, *37*, 785–789.
(76) Schultz, N. E.; Zhao, Y.; Truhlar, D. G. *J. Phys. Chem. A* **2005**, *109*, 4388–4403.
(77) Rappe, A. K.; Casewit, C. J.; Colwell, K. S.; Goddard, W. A.; Skiff, W. M. *J. Am. Chem. Soc.* **1992**, *114*, 10024–10035.
(78) Saebo, S.; Tong, W.; Pulay, P. *J. Chem. Phys.* **1993**, *98*, 2170–2175.
(79) Schutz, M.; Hetzer, G.; Werner, H. J. *J. Chem. Phys.* **1999**, *104*, 5691–5705.
(80) Zhao, Y.; Truhlar, D. G. *Theor. Chem. Acc.* **2008**, *120*, 215–241.
(81) *Jaguar*, version 7.0; Schrodinger, LLC: New York, 2007.
(82) Wadt, W. R.; Hay, P. J. *J. Chem. Phys.* **1985**, *82*, 284–298.
(83) Höllwarth, A.; Böhme, M.; Dapprich, S.; Ehlers, A. W.; Gobbi, A.; Jonas, V.; Köhler, K. F.; Stegmann, R.; Veldkamp, A.; Frenking, G. *Chem. Phys. Lett.* **1993**, *208*, 237–240.
(84) Ehlers, A. W.; Böhme, M.; Dapprich, S.; Gobbi, A.; Höllwarth, A.; Jonas, V.; Köhler, K. F.; Stegmann, R.; Veldkamp, A.; Frenking, G. *Chem. Phys. Lett.* **1993**, *208*, 111–114.
(85) Harihara, P.; Pople, J. A. *Theor. Chim. Acta* **1973**, *28*, 213–222.
(86) Hehre, W. J.; Ditchfie, R; Pople, J. A. *J. Chem. Phys.* **1972**, *56*, 2257–2261.
(87) Barone, V.; Cossi, M. *J. Phys. Chem. A* **1998**, *102*, 1995–2001.
(88) Cossi, M.; Rega, N.; Scalmani, G.; Barone, V. *J. Comput. Chem.* **2003**, *24*, 669–681.
(89) Tomasi, J.; Persico, M. *Chem. Rev.* **1994**, *94*, 2027–2094.
(90) Reed, A. E.; Curtiss, L. A.; Weinhold, F. *Chem. Rev.* **1988**, *88*, 899–926.
(91) Weinhold, F.; Landis, C. *Valency and Bonding A Natural Bond Orbital Donor-Acceptor Perspective*; Cambridge University Press: Cambridge, U. K., 2005.
(92) The LACV3P basis set is a triple-ζ contraction of the LACVP basis set developed and tested at Schrödinger, Inc.

been described by the 6-31G(d,p) basis set and hydrogen atoms by the 6-31G basis set.

Acknowledgment. This work was supported by the Spanish MICINN (DGI)/FEDER (Projects CTQ2008-06669-C02-01, CTQ2008-06866-C02-01 and Consolider Ingenio 2010 CSD2007-00006) and the Gobierno de Aragón (Grupo de Excelencia: Química Inorgánica y de los Compuestos Organometálicos). We thank Prof. P. Mastrorilli and Dr. V. Gallo (Dipartimento di Ingegneria delle Acque e di Chimica, Politecnico di Bari, Italy) for some NMR experiments and helpful discussions.

Supporting Information Available: Further details of the structure determinations of **2**[ClO_4]·2.5CH_2Cl_2, **5**[ClO_4]·4CH_2Cl_2, and **6**[ClO_4]·2.5CH_2Cl_2 including atomic coordinates, bond distances and angles, and thermal parameters. Relative energies at the BLYP and MP2 levels of the different isomers of **2** considered for the reduced system, selected geometrical parameters of all of the minima obtained with reduced (**r**) and complete (**c**) model systems, optimized structures of all of the minima obtained with the reduced model and Cartesian coordinates, and total energies of the optimized structures reported in the text. This material is available free of charge via the Internet at http://pubs.acs.org.